J. Fluid Mech. (2012), *vol.* 710, *pp.* 166–194.
doi:10.1017/jfm.2012.358

Asymptotic calculation of the dynamics of self-sustained detonations in condensed phase explosives

J. A. Saenz[1]†, B. D. Taylor[2] and D. S. Stewart[3]

[1] Research School of Earth Sciences, Australian National University, Canberra, ACT 0200, Australia

[2] Naval Research Laboratory, Washington, DC 20375-5344, USA

[3] Department of Mechanical Science and Engineering, University of Illinois at Urbana-Champaign, Urbana, IL 61801, USA

(Received 13 February 2012; revised 20 May 2012; accepted 9 July 2012;
first published online 31 August 2012)

We use the weak-curvature, slow-time asymptotics of detonation shock dynamics (DSD) to calculate an intrinsic relation between the normal acceleration, the normal velocity and the curvature of a lead detonation shock for self-sustained detonation waves in condensed phase explosives. The formulation uses the compressible Euler equations for an explosive that is described by a general equation of state with multiple reaction progress variables. The results extend an earlier asymptotic theory for a polytropic equation of state and a single-step reaction rate model discussed by Kasimov (Theory of instability and nonlinear evolution of self-sustained detonation waves. PhD thesis, University of Illinois Urbana-Champaign, Urbana, Illinois) and by Kasimov & Stewart (*Phys. Fluids*, vol. 16, 2004, pp. 3566–3578). The asymptotic relation is used to study the dynamics of ignition events in solid explosive PBX-9501 and in porous PETN powders. In the case of porous or powdered explosives, two composition variables are used to represent the extent of exothermic chemical reaction and endothermic compaction. Predictions of the asymptotic formulation are compared against those of alternative DSD calculations and against shock-fitted direct numerical simulations of the reactive Euler equations.

Key words: detonation waves, detonations

1. Introduction

The theory of detonation shock dynamics (DSD) considers the quasisteady propagation of self-sustained detonations in explosives, where the detonation structure is composed of a lead shock that initiates the reaction and ends at a point of sonic flow within the reaction zone. DSD theory is based on two asymptotic approximations: (i) the radius of curvature of the detonation shock is large compared with the thickness of the supporting reaction zone; and (ii) the rate at which the shock velocity or curvature changes is slow compared with the transit time of a material element through the reaction zone. In these asymptotic limits, approximate relationships between the curvature of the shock and its kinematics can be determined. A basic result is that the normal detonation velocity D is a function of the total curvature

† Email address for correspondence: juan.saenz@anu.edu.au

of the shock front κ, and this function depends only on the material properties of the explosive. In most DSD formulations, transverse variations along the shock are neglected.

An intrinsic relation between the normal shock velocity and curvature, the 'D–κ relation', was first given in Stewart & Bdzil (1988) for a case where D was close to the planar Chapman–Jouguet (CJ) detonation velocity. Since that time, D–κ relations have been obtained by analytical, numerical and asymptotic methods using a variety of equations of state and reaction rate models. It is an intrinsic material property used to characterize explosives and has been measured experimentally (Lambert *et al.* 2006). The D–κ relation is used in engineering applications to compute the time of arrival and changes in shock strength as detonations propagate through devices with complex geometries. When D is plotted as a function of κ, with $\kappa > 0$ representing a convex shock shape, the D–κ relation may be Z-shaped, with an upper, middle and a lower branch connected by turning points, or D may monotonically decrease with increasing κ. Asymptotic analyses that relate D, κ, their first and second time derivatives and their transverse spatial derivatives have been carried out for a model with an ideal equation of state and a single-step reaction. A complete description of DSD theory and applications can be found in Yao & Stewart (1996) and Stewart & Yao (1998), and in the reviews by Bdzil & Stewart (2007, 2011).

The governing equations, boundary conditions and other basic definitions used in this work are described in § 2. In § 3, asymptotics are used to derive an intrinsic relation between the normal acceleration $\dot{D}$, normal velocity D and total curvature κ of a detonation shock for a general equation of state that includes multiple reaction progress variables. These results complete calculations first proposed by Kasimov (2004), who obtained a $\dot{D}$–D–κ relation using an ideal equation of state with a single progress variable and suggested that the methodology could be extended to condensed phase explosives with more general equations of state. The analysis was not complete, but provided invaluable guidance. Section 5 describes the numerical algorithm used to solve the intrinsic $\dot{D}$–D–κ relation, and in § 6 the formulation proposed in this work is used to model condensed phase explosives with varied and simultaneous chemical and physical processes present, such as exothermic reaction and endothermic compaction, using the material models described in § 4.

2. Governing equations

This section introduces basic definitions, governing equations and boundary conditions that will be used in the asymptotic formulation of an intrinsic $\dot{D}$–D–κ relation for condensed phase explosives.

2.1. *Basic definitions*

Several basic definitions and relations are used in the asymptotic DSD formulation as well as in its numerical solution. They include concepts such as the properties of a self-sustained detonation, shock-attached coordinates, and conversion between state variables and flux variables.

2.1.1. *Self-sustained detonations*

Kasimov & Stewart (2004) showed that there is a characteristic surface, or information separatrix, that defines the end of the domain that affects the dynamics of an unsteady detonation front. The dynamics of self-sustained curved detonations depend only on the flow within a finite subsonic region between the shock and the trailing sonic locus. A planar, steady, self-sustained detonation wave travels at the Chapman–Jouguet speed D_{CJ}. In such a wave, the sonic locus is a characteristic

surface coincident with the end of the reaction zone. Overdriven detonations travel faster than D_{CJ} and are sustained by an external mechanism, such as a piston, so they are not considered here. The flow behind the shock is subsonic relative to the shock, meaning that acoustic disturbances can reach the shock. The reaction zone between the shock and sonic locus can be divided into two regions which have differing mathematical characteristics. The main reaction layer (MRL) is the region in the reaction zone that is immediately behind the shock front. The region of the reaction zone where the transition from subsonic flow to the sonic locus occurs is referred to as the transonic layer (TSL).

2.1.2. *Shock-attached coordinate frame*

The shock location in the laboratory frame is expressed as $r = R(t)$. The shock speed normal to the front is $D = R_t$ and the shock acceleration is $\dot{D} = D_t$, where subscript t indicates differentiation with respect to time. The normal distance from the shock surface,

$$n = r - R(t), \tag{2.1}$$

serves to define the fluid velocity relative to the shock as

$$U = u - D, \tag{2.2}$$

where u is the particle velocity in the laboratory frame. The shock curvature κ is given by

$$\kappa = j/R(t), \tag{2.3}$$

where $j = 0, 1$ or 2 for planar, cylindrical or spherical coordinates, respectively. Diverging (convex shape) and converging (concave shape) detonation waves have $\kappa > 0$ and $\kappa < 0$, respectively.

2.1.3. *State and flux variables*

The state of a material at any given point n in the reaction zone will be represented by pressure p, density ρ, specific volume $v = 1/\rho$, velocity in the shock-attached frame U and specific internal energy e. The composition variables Z_i represent scalar quantities to account for a general range of phenomena, such as chemical reactions, through mass fractions of chemical species or reaction progress variables, and compaction, through volume fraction or porosity. We assume the existence of a material model that consists of an incomplete equation of state for the specific internal energy of the general form $e(p, v, Z_i)$, and an expression for the time rate of change of composition variable Z_i as a function of the state of the material, $\omega_i(p, v, Z_j)$. Specific material models with this general form are given in § 4.

The mass flux M, momentum flux P and energy flux H for fixed Z_i are defined in terms of the state variables as

$$M = \rho\, U, \tag{2.4a}$$

$$P = p + \rho\, U^2, \tag{2.4b}$$

$$H = e + p\, v + \tfrac{1}{2}U^2. \tag{2.4c}$$

For a given set of flux variables M, P and H for fixed Z_i one can solve the defining algebraic relation to find state variables p, v and U. Solving for v and p in terms of U from definitions (2.4*a*,*b*) produces

$$v = \frac{U}{M}, \tag{2.5a}$$

$$p = P - MU. \tag{2.5b}$$

Using the above relations in the definition of the energy flux (2.4*c*) yields

$$e(p, v, Z_i) + \frac{(P - MU)U}{M} + \frac{1}{2}U^2 = H. \tag{2.6}$$

After solving (2.6) for U, v and p are found using (2.5*a*) and (2.5*b*), respectively. Alternatively, one can rewrite (2.6) in terms of v, resulting in

$$e(p, v, Z_i) + (P - M^2 v)v + \tfrac{1}{2}M^2 v^2 = H. \tag{2.7}$$

The difficulty in solving (2.6) for U or (2.7) for v depends on the form of the equation of state $e(p, v, Z_i)$. The ideal equation of state produces a quadratic equation that can be solved analytically, but in general the equation must be solved numerically. Section 4 presents specific examples of this solution for the applications to porous pentaerythritol tetranitrate (PETN) and PBX-9501.

2.2. *Reduced Euler equations*

Writing the reactive Euler equations for radially symmetric flow in the shock-attached frame using the definitions in (2.1)–(2.3) and expanding and truncating to leading-order in curvature κ, one obtains

$$M_n = -\rho_t - \kappa\rho(U + D), \tag{2.8a}$$

$$P_n = -M_t - \rho D_t - \kappa\rho U(U + D), \tag{2.8b}$$

$$H_n = -\frac{1}{U}H_t - D_t + \frac{1}{M}p_t, \tag{2.8c}$$

$$Z_{in} = -\frac{1}{U}Z_{it} + \frac{\omega_i}{U}. \tag{2.8d}$$

Equations (2.8*a–d*), referred to as the reduced Euler equations, constitute a system of equations for the flux variables M, P, H and composition variables Z_i as a function of time t and distance from the shock n in terms of curvature κ and detonation speed D.

2.3. *Boundary conditions at the shock*

The Rankine–Hugoniot relations dictate that the fluxes M, P and H are constant across the shock. The composition variables Z_i are also constant across the shock because the shock is treated as a discontinuity. We use subscripts s and 0 to denote variables at the shock and in the ambient state, respectively. Fluxes from the ambient material M_0, P_0 and H_0 for a wave moving at speed D can be calculated using the definitions in (2.4*a–c*) and the ambient state p_0, v_0, $u_0 = 0$, $U_0 = -D$, Z_{i0}. The fluxes and composition variables at the shock are given by

$$M_s = -\rho_0 D, \tag{2.9a}$$

$$P_s = p_0 + \rho_0 D^2, \tag{2.9b}$$

$$H_s = e_0 + p_0 v_0 + \tfrac{1}{2}D^2, \tag{2.9c}$$

$$Z_{is} = Z_{i0}. \tag{2.9d}$$

After solving for the velocity at the shock U_s in (2.6), v_s and p_s can be calculated using (2.5*a,b*).

2.4. *Boundary conditions at the sonic locus*

At the sonic locus ($n = n_*$) the flow is characteristic, meaning that the region between the sonic locus and the shock is acoustically isolated from the flow outside this region,

as shown by Kasimov & Stewart (2004). Subscript $*$ is used to indicate evaluation at the sonic locus. The state at the sonic locus obeys the C_+ characteristic equation

$$\frac{\mathrm{d}p_*}{\mathrm{d}t} + \rho_* c_* \frac{\mathrm{d}u_*}{\mathrm{d}t} + \kappa \rho_* c_*^2 u_* = \rho_* c_*^2 \sum_{i=1}^{N} \sigma_i \omega_i \tag{2.10}$$

on

$$\frac{\mathrm{d}n_*}{\mathrm{d}t} = c_* + U_*, \tag{2.11}$$

where the thermicity coefficient σ_i for composition variable i is defined as

$$\sigma_i = -\frac{1}{\rho c^2} \frac{\partial e/\partial Z_i}{\partial e/\partial p}, \tag{2.12}$$

and the sound speed is given by

$$c^2 = \frac{p + \partial e/\partial v}{\rho^2 \partial e/\partial p}. \tag{2.13}$$

Equation (2.10) and (2.11) are also referred to as the compatibility condition and the speed relation, respectively, and are used to define the state at the sonic locus. The reduced Euler equations (2.8*a–d*), along with the boundary conditions at the shock (2.9*a–d*) and the boundary conditions at the sonic locus (2.10)–(2.11), form a closed system of equations that fully describe the state profile $\{p(n), v(n), U(n), Z_i(n) : n_* \geqslant n \geqslant 0\}$ of a self-sustained detonation wave with curvature κ, travelling at speed D, in the limit of small shock curvature.

3. Calculation of an intrinsic $\dot{D}$–D–κ relation

The asymptotic analysis can be summarized as follows. Matched asymptotic expansions of the reduced Euler equations in the MRL and the TSL are used to find expressions for mass, momentum and energy fluxes, and their corresponding state variables. Transverse spatial variations along the shock are neglected. The expansion in the shock-attached frame of the MRL uses the planar quasisteady solution at the shock obtained from the Rankine–Hugoniot algebra as the leading-order solution. The expansion in the sonic frame for the TSL uses the sonic state as the leading-order solution. Similar to the approach used by Kasimov (2004) and Kasimov & Stewart (2005), the planar quasisteady solution ($\dot{D} = 0$ and $\kappa = 0$) of the reduced Euler equations at an arbitrary value of D, not necessarily close to D_{CJ}, is used as the leading-order solution in the expansions. Away from the sonic locus, the solution from the expansion in the TSL is matched to the expansion in the MRL away from the shock. The matching of the MRL and TSL solutions provides expressions for the state in the reaction zone, to leading order in $\dot{D}$ and κ, that are used to enforce the boundary conditions at the sonic locus, leading to expressions that relate $\dot{D}$, D and κ. The boundary conditions at the sonic locus are then enforced to leading order in $\dot{D}$ and κ, resulting in an intrinsic $\dot{D}$–D–κ relation for the dynamics of a detonation wave.

3.1. *Planar quasisteady solution*

The starting point is the planar quasisteady solution, which serves as the leading-order solution for the asymptotic expansions. The planar quasisteady solution is obtained by setting the curvature and all time derivatives to zero in the reduced Euler equations (2.8*a–d*). As a result, the fluxes are constant throughout the reaction zone, and are

given by the boundary conditions at the shock (2.9*a–c*) as a function of D. At the sonic locus the compatibility condition and the speed relation for a planar quasisteady shock become

$$\rho_* c_*^2 \sum_{i=1}^{N} \sigma_{i*}\omega_{i*} = 0, \tag{3.1a}$$

$$c_* + U_* = 0. \tag{3.1b}$$

Quantities obtained from the planar quasisteady solution will be denoted by subscript (0). Integrating (2.8*d*) in n from the shock ($n = 0$) to the far field until (3.1*a,b*) are satisfied results in a spatial profile $Z_{i(0)}(n)$ and gives $n_{(0)*}$. Using $Z_{i(0)}(n)$ and the fluxes at the shock (2.9*a–c*), (2.5*a,b*) and (2.6) are solved for $p(n)$, $v(n)$ and $U(n)$, yielding $U_{(0)}(n)$, $p_{(0)}(n)$ and $v_{(0)}(n)$. As a result, we obtain profiles $p_{(0)}(n)$, $v_{(0)}(n)$, $U_{(0)}(n)$ and $Z_{i(0)}(n)$ between the shock and the sonic locus that only depend on the detonation speed D.

3.2. *Asymptotic expansions*

The reduced Euler equations (2.8*a–d*) are integrated in the MRL from the shock through the reaction zone to obtain the following set of integral equations in the flux variables

$$M = M_{(0)} + M_I, \tag{3.2a}$$

$$P = P_{(0)} + P_I, \tag{3.2b}$$

$$H = H_{(0)} + H_I, \tag{3.2c}$$

$$Z_i = Z_{i0} + Z_{iI}, \tag{3.2d}$$

with

$$M_I = -\int_0^n \frac{\partial \rho}{\partial t}\,\mathrm{d}n - \kappa \int_0^n \rho(U + D)\,\mathrm{d}n, \tag{3.3a}$$

$$P_I = -\int_0^n \left(\frac{\partial M}{\partial t} + \rho\dot{D}\right)\mathrm{d}n - \kappa \int_0^n \rho U(U + D)\,\mathrm{d}n, \tag{3.3b}$$

$$H_I = \int_0^n \left(-\frac{H_t}{U} - \dot{D} + \frac{p_t}{M}\right)\mathrm{d}n, \tag{3.3c}$$

$$Z_{iI} = \int_0^n \frac{\omega_i - (Z_i)_t}{U}\,\mathrm{d}n, \tag{3.3d}$$

where $M_{(0)}$, $P_{(0)}$, $H_{(0)}$ correspond to the quasisteady planar fluxes and Z_{i0} is the composition at the shock. Note that $M_{(0)} = M_0$, $P_{(0)} = P_0$, $H_{(0)} = H_0$ and are constant throughout the reaction zone. No approximations to the reduced Euler equations (2.8*a–d*) were made in deriving the integral equations (3.3*a–d*). For slow time variation and small curvature, M_I, P_I, H_I and Z_{iI} correspond to asymptotically small corrections to the planar quasisteady fluxes and to the composition at the shock, respectively.

In the TSL the reduced Euler equations (2.8*a–d*) are written in a coordinate frame attached to the sonic locus. A spatial variable in this coordinate frame, N, is defined as the distance from the sonic locus normal to the shock, $N = n - n_*(t)$. Defining $\mathscr{D}$ as the normal speed of the sonic locus with respect to the lab frame, the particle velocity relative to the sonic locus is $\mathscr{U} = u - \mathscr{D}$. Integrating from the sonic locus towards the far field in the reaction zone results in a set of equations similar to (3.2*a–d*), where

the boundary conditions at the sonic locus are used to determine the leading-order solution, denoted by the subscript *,

$$\mathscr{M}[\equiv \rho\,\mathscr{U}] = \mathscr{M}_* + \mathscr{M}_I, \tag{3.4a}$$

$$\mathscr{P}\left[\equiv p + \rho\,\mathscr{U}^2\right] = \mathscr{P}_* + \mathscr{P}_I, \tag{3.4b}$$

$$\mathscr{H}\left[\equiv e + pv + \tfrac{1}{2}\mathscr{U}^2\right] = \mathscr{H}_* + \mathscr{H}_I, \tag{3.4c}$$

$$\mathscr{Z}_i = \mathscr{Z}_{i*} + \mathscr{Z}_{iI}. \tag{3.4d}$$

The flux variables $\mathscr{M}$, $\mathscr{P}$ and $\mathscr{H}$ are defined in the same manner as (2.4a–c) and $\mathscr{Z}_i$ is used to denote the composition variables in the TSL. Corrections to the leading-order solutions are defined as

$$\mathscr{M}_I = -\int_0^N \frac{\partial \rho}{\partial t}\,\mathrm{d}N - \kappa \int_0^n \rho(\mathscr{U} + \mathscr{D})\,\mathrm{d}N, \tag{3.5a}$$

$$\mathscr{P}_I = -\int_0^N \left(\frac{\partial \mathscr{M}}{\partial t} + \rho\dot{\mathscr{D}}\right)\mathrm{d}N - \kappa \int_0^N \rho\,\mathscr{U}(\mathscr{U} + \mathscr{D})\,\mathrm{d}N, \tag{3.5b}$$

$$\mathscr{H}_I = \int_0^N \left(-\frac{\mathscr{H}_t}{\mathscr{U}} - \dot{\mathscr{D}} + \frac{p_t}{\mathscr{M}}\right)\mathrm{d}N, \tag{3.5c}$$

$$\mathscr{Z}_{iI} = \int_0^N \frac{\omega_i - (\mathscr{Z}_i)_t}{\mathscr{U}}\,\mathrm{d}N. \tag{3.5d}$$

Matching the expansions in the TSL and the MRL is done in exactly the same manner as in Kasimov & Stewart (2005) and yields two important conclusions that will be used in our calculations. First, to leading order, the expansions for the state variables at the sonic locus in the shock-attached frame depend only on D. Owing to the time derivatives in the compatibility condition (2.10), only the leading-order solution is needed to enforce the compatibility condition to $O(\dot{D}, \kappa)$. Using the chain rule to find the time derivatives in terms of derivatives with respect to D, we get

$$\dot{D}\left[\frac{\mathrm{d}p_{(0)*}}{\mathrm{d}D} + \rho_{(0)*}c_{(0)*}\frac{\mathrm{d}u_{(0)*}}{\mathrm{d}D}\right] + \kappa\rho_{(0)*}c_{(0)*}^2 u_{(0)*} = \rho_{(0)*}c_{(0)*}^2 \sum_{i=1}^{N} \sigma_{i(0)*}\omega_{i(0)*}, \tag{3.6}$$

which can be rewritten as

$$\dot{D} = \frac{\rho_{(0)*}c_{(0)*}^2 \displaystyle\sum_{i=1}^{N} \sigma_{i(0)*}\omega_{i(0)*} - \kappa\rho_{(0)*}c_{(0)*}^2 u_{(0)*}}{\dfrac{\mathrm{d}p_{(0)*}}{\mathrm{d}D} + \rho_{(0)*}c_{(0)*}\dfrac{\mathrm{d}u_{(0)*}}{\mathrm{d}D}}. \tag{3.7}$$

Matching the MRL and the TSL expansions leads to a second conclusion, that the magnitude of the relative velocity of the sonic locus with respect to the shock, $\dot{n}_*$, is smaller than $O(\dot{D}, \kappa)$, and $\dot{n}_*$ can be neglected when the speed relation (2.11) is evaluated to $O(\dot{D}, \kappa)$, leading to

$$c_* + U_* = 0. \tag{3.8}$$

Approximations to M_I, P_I, H_I and Z_{iI} are found by expanding the integrands in (3.2a–d) around the planar quasisteady solution, leading to correction terms $M_{(1)}$, $P_{(1)}$, $H_{(1)}$ and $Z_{i(1)}$ to the planar quasisteady terms. Then the fluxes at the sonic locus are

evaluated to $O(\dot{D}, \kappa)$ using a modified version of equations (3.2*a–d*), resulting in

$$M_* = M_{(0)*} + M_{(1)*}, \tag{3.9a}$$
$$P_* = P_{(0)*} + P_{(1)*}, \tag{3.9b}$$
$$H_* = H_{(0)*} + H_{(1)*}, \tag{3.9c}$$
$$Z_{i*} = Z_{i(0)*} + Z_{i(1)*}, \tag{3.9d}$$

where terms $M_{(0)*}$, $P_{(0)*}$, $H_{(0)*}$ and $Z_{i(0)*}$ are obtained as described in § 2.3. The correction terms are given by

$$M_{(1)*} = -\dot{D}I_1 - \kappa M_{(0)*} n_{(0)*} - \kappa D I_0, \tag{3.10a}$$
$$P_{(1)*} = \rho_0 \dot{D} n_{(0)*} - \dot{D} I_0 - \kappa M_{(0)*}^2 J_0 - \kappa M_{(0)*} D n_{(0)*}, \tag{3.10b}$$
$$H_{(1)*} = \frac{-D\dot{D}I_0}{M_{(0)*}} - \dot{D} n_{(0)*} + \frac{\dot{D} S_1}{M_{(0)*}}, \tag{3.10c}$$
$$Z_{i(1)*} = -\dot{D}T_i - \frac{\dfrac{\partial Z_{i(0)*}}{\partial D}}{U_{(0)*}} \dot{D} n_{(1)*}, \tag{3.10d}$$

where

$$I_0 = \int_0^{n_{(0)*}} \rho_{(0)} \, \mathrm{d}n, \tag{3.11a}$$
$$J_0 = \int_0^{n_{(0)*}} v_{(0)} \, \mathrm{d}n, \tag{3.11b}$$
$$I_1 = \int_0^{n_{(0)*}} \frac{\partial \rho_{(0)}}{\partial D} \, \mathrm{d}n, \tag{3.11c}$$
$$S_1 = \int_0^{n_{(0)*}} \frac{\partial p_{(0)}}{\partial D} \, \mathrm{d}n, \tag{3.11d}$$
$$T_i = \int_0^{n_{(0)*}} \frac{1}{U_{(0)}} \frac{\partial Z_{i(0)}}{\partial D} \, \mathrm{d}n, \tag{3.11e}$$

where we have used the expansion $n_* = n_{(0)*} + n_{(1)*} + \cdots$ to obtain the above equations. The term $n_{(1)*}$ is a measure of the deviation of n_* from $n_{(0)*}$, and is related to $\dot{n}_*$. We will postpone finding an expression for $n_{(1)*}$ for the time being. Note that I_0, J_0, I_1, S_1 and T_i only depend on the planar quasisteady solution, which is a function of D. Here $M_{(1)}$, $P_{(1)}$, $H_{(1)}$ and $Z_{i(1)}$ are functions of $\dot{D}$, D, κ. In general, $Z_{i(1)}$ is also a function of $\dot{n}_*$.

Fluxes at the sonic locus M_*, P_*, H_* and Z_{i*} are obtained by evaluating (3.9*a–d*) at $n_{(0)*}$ and are linear in $\dot{D}$ and κ. The state at the sonic locus (U_*, v_*, p_*) is then obtained by solving (2.6) and (2.5*a,b*), using M_*, P_*, H_* and Z_{i*}. With the state at the sonic locus defined, the compatibility condition (3.7) and the speed relation (3.8) form a system of equations in $\dot{D}$, D, κ and $\dot{n}_*$ that can be solved to obtain the $\dot{D}$–D–κ relation for a given material model.

For the special case of a material model that uses an ideal equation of state and a single reaction progress variable with an Arrhenius reaction rate equation, (2.6) and (2.5*a,b*) can be solved analytically to obtain truncated expressions for U_*, v_*, p_* to $O(\dot{D}, \kappa)$ (Kasimov & Stewart 2005). If instead these equations are solved numerically, higher-order terms are not truncated and more accurate values for U_*, v_*, and p_* are

obtained. Using the state at the sonic locus calculated numerically one can obtain a more accurate $\dot{D}$–D–κ relation than using the state at the sonic locus obtained analytically and truncated to $O(\dot{D}, \kappa)$. In general, however, substituting the equation of state into (2.6) and (2.5*a*,*b*) will not produce a system of equations that can be solved analytically, and the solution can only be obtained numerically.

3.3. *Properties of the expansions*

The nature of the expansions of the flux variables and the state variables for an ideal equation of state is described in Kasimov (2004) and Stewart & Kasimov (2005). Using an ideal equation of state $e = pv/(\gamma - 1) - Z_1 Q$, where γ is the polytropic exponent and Q is the heat of reaction, and a single reaction progress variable Z_1, the energy equation (2.7) is a quadratic in v that can be solved to give

$$v = \frac{\gamma}{\gamma + 1} \frac{P}{M^2} (1 - \delta), \tag{3.12}$$

where the discriminant δ is given by

$$\delta = \sqrt{1 - \frac{2(\gamma^2 - 1)}{\gamma^2} \frac{M^2}{P^2} (H + Z_1 Q)}. \tag{3.13}$$

The properties of the discriminant can be used to explain the nature of the expansions in the MRL and in the TSL. The root of δ on the compression branch is a regular function of the arguments in the square root on the right-hand side of (3.13). At the sonic locus the discriminant has a single root which is a local minimum. The expansion in the TSL is regular because the state at the sonic locus is used as the leading-order solution. In the MRL on the other hand, expansion of the discriminant produces terms that are inversely proportional to powers of the argument of the square root in (3.13). The order of the expansion changes near the sonic locus, where the discriminant is zero. Similarly, as one approaches the sonic locus, expansions for the state variables in the MRL become irregular. This irregularity is resolved by matching the expansion in the MRL with the expansion in the TSL.

Monotonicity of the isentropes in the p–v plane for any consistent equation of state means that in general (2.7) will have a quadratic character. See Menikoff & Plohr (1989) for a review of the thermodynamic properties of equations of state. In the present work, the formulation by Kasimov (2004) and Stewart & Kasimov (2005) is generalized to thermodynamically consistent equations of state. The properties of the discriminant (3.13) at the sonic locus, namely that it has a single root and that this root is a minimum, dictates the choice of the numerical algorithm used to solve for the state at the sonic locus.

4. Material models

In this section we describe the material models that will be studied using our asymptotic DSD formulation. Each model consists of an equation of state and a rate equation for chemical reaction. Some models also include a rate equation for compaction. The progress of an exothermic chemical reaction will be tracked with the composition variable Z_1. The volume fraction Z_2 of solid reactants in a representative volume element will represent the endothermic process of compaction in the material. Constitutive forms for the equation of state $e(p, v, Z_i)$ are supplied to account for the effects of reaction and compaction in the energy budgets in the material.

4.1. *Reaction models*

A single-step exothermic chemical reaction with a reaction progress variable $Z_1 \equiv \lambda$ will be used to track reaction progress, where $\lambda = 0$ in unreacted material and $\lambda = 1$ in fully reacted material. We consider two reaction rate models commonly used in detonation theory: an Arrhenius rate and a pressure-dependent rate.

The Arrhenius rate equation is given by

$$\omega_\lambda = k_\lambda\,(1-\lambda)^\nu \exp\left[\frac{-E_a}{pv}\right], \tag{4.1}$$

where k_λ is the rate constant, ν is the depletion factor and E_a is the activation energy.

The pressure-dependent reaction rate equation is

$$\omega_\lambda = k_\lambda\,(1-\lambda)^\nu \left(\frac{p}{p_{CJ}}\right)^N, \tag{4.2}$$

where p_{CJ} is the Chapman–Jouguet pressure and N is the pressure exponent.

For high activation energy E_a or high pressure exponent N, the reaction rate given by the Arrhenius or pressure-dependent rate changes rapidly with changes in the state $(p,\ v,\ \lambda)$. In those cases the assumption that ω_λ is $O(\dot{D}, \kappa)$ in the compatibility condition (3.7) is satisfied since the reaction rate is small by virtue of the rate form. Reaction rates calculated with the Arrhenius and the pressure-dependent rate equations are continuous in the interval $0 \leqslant \lambda \leqslant 1$.

4.2. *Compaction models*

The compaction progress in solid–void explosives is represented by variable $Z_2 \equiv \phi$, defined as the ratio of the volume of solids to the total volume in a representative volume element. For a fully compacted explosive $\phi = 1$ and for explosive beds that are not fully compacted $\phi_0 \leqslant \phi \leqslant 1$, where $\phi_0 > 0$ is the initial compaction of the bed. Compaction is the net endothermic increase in density of a representative volume element associated with pore volume reduction by processes such as grain rearrangement, grain deformation and fracture of solids.

Stewart, Asay & Prasad (1994) described a simple model in which the compaction rate is represented by a linear quasistatic process. Based on this model, we will use a rate of compaction given by

$$\omega_\phi = k_\phi \tanh[100(1-\phi)](Ap - \phi) \quad \text{with } A = \phi_0/p_0, \tag{4.3}$$

where the term $\tanh[100(1-\phi)]$ is included to ensure that the compaction rate continuously and smoothly goes to zero as ϕ goes to one.

Xu & Stewart (1997) modelled dynamic compaction of a bed of porous material under pressure loading by using a P–α model (Herrmann 1969). The rate of compaction is due to a deviation of the bed pressure from the pressure realized by an isothermal quasistatic response of the porous reactant solid of the form

$$p_{eqb} = p_0 + \mathscr{P}(\phi), \tag{4.4}$$

where p_{eqb} is the volume average pressure in the porous solid, p_0 is the initial pressure at $\phi = \phi_0$ and $\mathscr{P}(\phi)$ is called the 'configurational stress'. The configurational stress dependence usually is determined from quasistatic compaction experiments. The experimentally determined quasistatic bed pressure to porosity $(\alpha \equiv 1/\phi)$ response can

be fit with a quadratic P–α relation,

$$\frac{\alpha - 1}{\alpha_0 - 1} = \left(1 - \frac{\mathscr{P}(\phi)}{P_h}\right)^2, \tag{4.5}$$

where the parameter P_h is called the hardening pressure, or consolidation pressure, for bed pressures above which the porous material will crush to solid density. The compaction rate is assumed to be proportional to the difference between the average pressure in the bed p and the equilibrium pressure p_{eqb}, i.e. $p - p_{eqb}$. This assumption, along with (4.5), gives

$$\omega_\phi = k_\phi \tanh[100(1-\phi)]\left[p - p_0 - P_h\left(1 - \sqrt{\frac{\phi_0(1-\phi)}{\phi(1-\phi_0)}}\right)\right]. \tag{4.6}$$

The parameter k_ϕ derives from consideration of dynamic relaxation processes in the bed, and its value reflects the rise time to achieve a given state of compaction when the porous material is impacted by a constant velocity piston.

4.3. *Equations of state*

4.3.1. *Ideal equation of state*

The simplest approach to model the effects of reaction and compaction on the constitutive behaviour of an energetic material is to use the ideal equation of state for a polytropic gas, with terms to account for the energy released by the exothermic reaction process and the energy absorbed by the endothermic compaction process, resulting in

$$e = e(p, v, \lambda, \phi) = \frac{pv}{\gamma - 1} - Q_T, \tag{4.7}$$

where

$$Q_T = Q_\lambda \lambda + Q_\phi(1 - \phi), \tag{4.8}$$

γ is the polytropic exponent, Q_λ is the heat of reaction and Q_ϕ is the energy absorbed by compaction. The sound speed is given by $c = \sqrt{\gamma p v}$.

4.3.2. *Wide-ranging equation of state*

The wide-ranging equation of state (WR-EOS) was developed by Davis and coworkers in a series of papers (Davis 1985, 1993, 1998*a*,*b*, 2000; Stewart, Davis & Yoo 2002) to cover the wide range of states encountered in detonation problems. It is an empirically formulated equation of state, although developed with significant physical considerations. Recently, Wescott, Stewart & Davis (2005), Lambert *et al.* (2006), Stewart, Yoo & Wescott (2007) and Saenz & Stewart (2008) used the WR-EOS to develop models of condensed explosives that are capable of accurately predicting detonation dynamics for states outside the range of the calibration of the model. In what follows, the WR-EOS and the mixture closure conditions used in Saenz & Stewart (2008) are briefly described.

The WR-EOS uses the Mie–Grüneisen form for isolated phases, namely

$$e(p, v) = e^s(v) + \frac{v}{\Gamma(v)}(p - p^s(v)) \quad \text{or} \quad p(e, v) = p^s(v) + \frac{\Gamma(v)}{v}(e - e^s(v)). \tag{4.9}$$

We will use r and p subscripts to denote reactants and products, respectively. The superscript s represents the reference states, which are the isentrope that passes

through the CJ state for products and shock Hugoniot states for reactants. The forms of the equations for the reference values $p_p^s(v)$, $e_p^s(v)$ and $\Gamma_p(v)$ for the products and $p_r^s(v)$, $e_r^s(v)$ and $\Gamma_r(v)$ for the reactants may be found in Wescott *et al.* (2005) and are summarized in appendix A.

The energy equation of state for the mixture of porous solid (the mixture of condensed reactant and void, indicated by subscript *ps*) and products is a mass-weighted average of the energies in each phase. This leads to a mixture energy equation of state for the mixture of porous solid and products,

$$e(v, p, \lambda, \phi) = (1 - \lambda)e_r(p/\phi, v_r) + \lambda e_p(p, v_p). \tag{4.10}$$

The closure relations relate the pressure and specific volume in the different phases. Pressure equilibrium is enforced between the porous solid and the reaction products, such that

$$p_{ps} = p_p = p. \tag{4.11}$$

The pressure in the condensed reactant phase is higher and depends on the reactant volume fraction with $p_r = p/\phi$. The second closure condition specifies the ratio of specific volumes of reactants and products so that the mixture-specific volume is given by

$$v = (1 - \lambda)v_{ps} + \lambda v_p, \tag{4.12}$$

with

$$\Phi = v_{ps}/v_p \quad \text{and} \quad v_r = \phi v_{ps}. \tag{4.13}$$

Stewart *et al.* (2002) showed that the values of Φ vary between approximately 0.8 and 1.0 and that the sensitivity of the WR-EOS to Φ is low. They suggested that a good approximation is to set $\Phi = 0.95$ when $\lambda > 0$, and $\Phi = 1$ when $\lambda = 0$. Alternatively, at a high computational cost, one can enforce temperature equilibrium between phases, a condition used in Wescott *et al.* (2005). Equations (4.12) and (4.13) can be recast as

$$v_p = \frac{v}{[\lambda + (1 - \lambda)\Phi]}, \quad v_{ps} = \frac{\Phi v}{[\lambda + (1 - \lambda)\Phi]} \quad \text{and} \quad v_r = \frac{\phi\, \Phi\, v}{[\lambda + (1 - \lambda)\Phi]}. \tag{4.14}$$

When $\phi = 1$, the WR-EOS for powders described by Saenz & Stewart (2008) is consistent with the WR-EOS for fully solid condensed phase explosives used by Wescott *et al.* (2005).

The pressure equilibrium condition displayed in (4.11) can cause difficulties in some models, such as leading to ill-posed sets of equations. However, this does not happen here because (4.11) is only used to write a physically sensible equation of state for the bulk material $e(v, p, \lambda, \phi)$, and therefore the system of equations (2.8*a–d*) has a strictly hyperbolic character and it evolves on particle velocity characteristics.

5. Numerical solution of the asymptotically formulated $\dot{D}$–D–κ relation

This section describes a numerical procedure $\mathscr{F}(D, \kappa)$ to calculate $\dot{D}$ as a function of D and κ, $\dot{D} = \mathscr{F}(D, \kappa)$, from the asymptotically formulated compatibility condition (3.7) and speed relation (3.8). To implement $\mathscr{F}(D, \kappa)$ for a material model with a reaction progress variable $Z_1 \equiv \lambda$ and a compaction progress variable $Z_2 \equiv \phi$, (3.9)–(3.11) are transformed to λ coordinates, as shown in appendix B.

We start by defining the residual functions that are used to enforce (3.7) and (3.8) for use with a root solving scheme. The residual functions need to be calculated

reliably over a wide range of values for $\dot{D}$ and λ_* so that the root solve will succeed. To enforce the compatibility condition we rewrite (3.7) as

$$R_1 = \left(\frac{\mathrm{d}p_{(0)*}}{\mathrm{d}D} + \rho_{(0)*} c_{(0)*} \frac{\mathrm{d}u_{(0)*}}{\mathrm{d}D} \right) \dot{D} - \rho_{(0)*} c_{(0)*}^2 \sum_{i=1}^{N} \sigma_{i(0)*} \omega_{i(0)*} + \kappa \rho_{(0)*} c_{(0)*}^2 u_{(0)*}. \quad (5.1)$$

Here R_1 depends only on the leading-order solution, D, κ and an estimate for $\dot{D}$.

A robust and reliable residual function R_2 to enforce the speed relation (3.8) requires careful consideration of the character of the solution at the sonic locus. Define $(\dot{D}, \lambda_*)_A$ as a point that satisfies (3.8). Recalling the discussion in § 3.3, (2.6) has a single root when evaluated at the state corresponding to point $(\dot{D}, \lambda_*)_A$ and that root represents a minimum. Guesses in the neighbourhood of $(\dot{D}, \lambda_*)_A$ can be such that (2.6) has two real roots or no real roots. The solution point $(\dot{D}, \lambda_*)_A$ therefore lies on the edge of the region for which (3.8) is real valued, and a numerical scheme that uses a residual function based on (3.8) will be, at best, very slow to converge. For this reason, we define the following root function based on (2.6),

$$R_2 = \min(\mathscr{H}) \quad (5.2)$$

where

$$\mathscr{H} = H_* - e(p_*, v_*, \lambda_*, \phi_*) - \frac{(P_* - M_* U_*) U_*}{M_*} - \frac{1}{2} U_*^2. \quad (5.3)$$

The speed relation (3.8) is satisfied when $R_2 = 0$ as defined above. To find R_2, we use the Brent minimization algorithm implemented by Galassi *et al.* (2009).

The procedure to compute the asymptotic relation $\dot{D} = \mathscr{F}(D, \kappa)$ is:

(i) read D and κ;
(ii) calculate the leading-order state at the sonic locus, $p_{(0)*}$, $v_{(0)*}$, $U_{(0)*}$ and $Z_{i(0)*}$, using the method described in § 3.1;
(iii) using (2.9), calculate the leading-order solution to flux variables at the sonic locus $M_{(0)*}$, $P_{(0)*}$, $H_{(0)*}$;
(iv) using (B 3), calculate I_0, J_0, I_1, S_1 and T at the sonic locus;
(v) calculate $c_{(0)*}$, $\omega_{\lambda(0)*}$, $\omega_{\phi(0)*}$, $\sigma_{\lambda(0)*}$ and $\sigma_{\phi(0)*}$;
(vi) estimate $\dot{D}$ and λ_*;
(vii) using (B 1) and (B 2), calculate M_*, P_*, H_* and ϕ_* ;
(viii) calculate R_1 using (5.1) and R_2 using (5.2);
(ix) if R_1 and R_2 are larger than the desired tolerance, go to (vi).

6. Results and examples

In this section we present results of the asymptotic theory applied to the explosive materials models discussed in § 4. The numerical procedure $\mathscr{F}(D, \kappa)$ developed in § 5 is used to construct asymptotic D–κ relations and ignition curves. These results are compared against D–κ relations obtained by numerical solution of the quasisteady reduced Euler equations, referred to as 'numerical' D–κ relations. The algorithm used to calculate numerical D–κ relations is given in appendix C. Lastly, spherically symmetric expanding ignition events in a solid explosive are computed by solving $\dot{D} = \mathscr{F}(D, \kappa)$ as an initial value problem and compared with ignition transients from shock-fitted direct numerical simulations (DNSs) computed using the scheme of Taylor (2010).

6.1. $\dot{D}$–D–κ *relation for a porous explosive modelled with an ideal equation of state*

Kasimov & Stewart (2005) formulated a $\dot{D}$–D–κ relation analytically to $O(\dot{D}, \kappa)$ for a material modelled by an ideal equation of state and a single-step reaction. In this section, their results are extended to a detonation model that includes a compaction process.

Using the ideal equation of state (4.7) in (2.7) we obtain

$$v^2 - \frac{2\gamma}{\gamma+1}\frac{P}{M^2}v + \frac{2(H+Q_T)}{M^2}\frac{\gamma-1}{\gamma+1} = 0. \tag{6.1}$$

Solving the above quadratic equation in v and using the physically relevant root,

$$v = \frac{\gamma}{\gamma+1}\frac{P}{M^2}\left(1-\delta\right), \tag{6.2}$$

where the discriminant δ is given by

$$\delta^2 = 1 - \frac{2(\gamma^2-1)}{\gamma^2}\frac{M^2}{P^2}\left(H+Q_T\right). \tag{6.3}$$

Using the Mach number in the shock-attached frame

$$\mathsf{M}^2 = \frac{U^2}{c^2}, \tag{6.4}$$

we can rewrite the discriminant δ in (6.3) as

$$\delta^2 = \left(\frac{1-\mathsf{M}^2}{1+\gamma\mathsf{M}^2}\right)^2. \tag{6.5}$$

Note that at the sonic locus where $\mathsf{M}=1$, the speed relation in (3.8) holds and the discriminant $\delta = 0$.

Matching the MRL and TSL expansions produces expressions for the leading-order sonic state that can be substituted into the compatibility condition and the speed relation. The resulting equation for the compatibility condition is

$$\dot{D} = a_1(Q_\lambda\omega_\lambda^* - Q_\phi\omega_\phi^*) - a_2\kappa, \tag{6.6}$$

where

$$a_1 = \frac{(\gamma^2-1)(\gamma+1)D^3}{(3D^2+c_0^2)(c_0^2+\gamma D^2)} \tag{6.7a}$$

and

$$a_2 = \frac{(c_0^2+\gamma D^2)(D^2-c_0^2)}{(\gamma+1)(3D^2+c_0^2)}. \tag{6.7b}$$

The resulting equation for the speed relation, to $O(\dot{D}, \kappa)$, is given by

$$G - \lambda_* Q_\lambda - (1-\phi_*)Q_\phi + Q_{T0} + \kappa x + \dot{D}y = 0, \tag{6.8}$$

where

$$G = \frac{(c_0^2-D^2)^2}{2(\gamma^2-1)D^2}, \tag{6.9a}$$

$$x = v_0\frac{(c_0^2+\gamma D^2)\gamma}{(\gamma^2-1)D}\int_0^{n_{(0)*}}\frac{p_{(0)}}{U_{(0)}}\left(1-\frac{v_{(0)}}{v_0}\right)\mathrm{d}n_{(0)} \tag{6.9b}$$

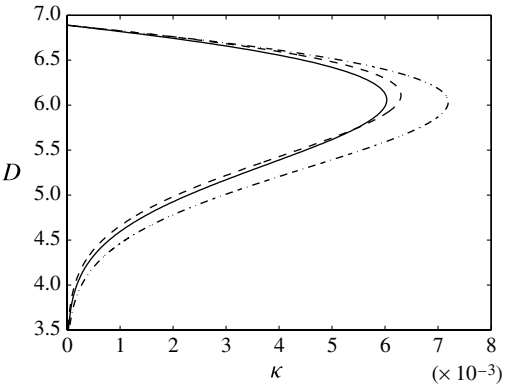

FIGURE 1. Comparison of non-dimensional D–κ relations for a hydrogen–oxygen mixture with $Q = 40$, $\gamma = 1.25$, $\nu = 1.0$ and $E = 40$. The dashed line is the solution to the asymptotic D–κ relation $\mathscr{F}(D, \kappa) = 0$. The solid line is the numerical D–κ relation and the dash-dot line is the relation obtained by solving the $\dot{D}$–D–κ relation for $\dot{D} = 0$ found in Kasimov & Stewart (2005).

and

$$y = \frac{D\,(\gamma+1)^2}{(\gamma^2-1)} \int_0^{n_{(0)*}} \frac{(1-v_r)}{U_{(0)}} \times \left[\frac{v_{(0)}}{v_{(0)*}-v_{(0)}} (v_r-\beta) \left(\frac{v_{(0)*}^2}{v_{(0)}^2} - \beta \right) + \frac{\gamma c_0^2 + D^2}{(\gamma+1)^2 D^2} + 2\beta\,(1-v_r) \right] \mathrm{d}n_{(0)}, \quad (6.10)$$

with

$$\beta = \frac{\gamma-1}{\gamma+1} \quad \text{and} \quad v_r = \frac{v_{(0)}}{v_0}. \quad (6.11)$$

The compatibility condition (6.6) and speed relation (6.8) are an asymptotic $\dot{D}$–D–κ relation for a porous explosive modelled with an ideal equation of state. Equation (6.6) shows that, to leading order, the dynamics of detonation waves are governed by competing mechanisms of acceleration caused by energy release from reaction and deceleration due to energy absorption from compaction and flow divergence. Equations (6.6) and (6.8) can also be obtained, after some tedious algebra, by substituting the ideal equation of state (4.7) into the compatibility condition (3.7) and the speed relation (3.8), and keeping only leading-order terms in $\dot{D}$ and κ. We use (6.6) and (6.8) to obtain D–κ relations that are compared with relations obtained using $\mathscr{F}(D, \kappa) = 0$.

6.2. *D–κ relations for a hydrogen–oxygen mixture*

We calculate the D–κ relation for a hydrogen–oxygen mixture using an ideal equation of state and an Arrhenius reaction rate, setting $Z_2 = \phi = 1$ (no compaction). Consider a mixture with $Q_\lambda = 40$, $\gamma = 1.25$, $\nu = 1.0$, $E = 40$ and $D_{CJ} = 6.8896$, which corresponds to the case shown in figure 5 of Kasimov & Stewart (2005), where the ambient state and the half-reaction length of a plane CJ detonation are used to scale parameters and variables. The resulting relation is shown in figure 1. We also show the D–κ relation calculated using the formulation by Kasimov & Stewart (2005), i.e. solving (6.6) and (6.8), and the numerical D–κ relation. The three curves display very

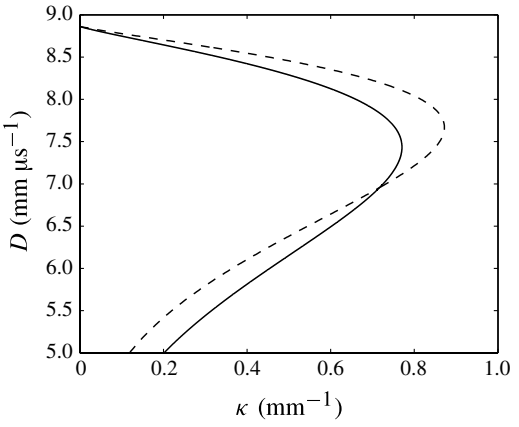

FIGURE 2. Comparison of D–κ relations for PBX-9501. The dashed line is the solution to the asymptotic D–κ relation $\mathscr{F}(D, \kappa) = 0$. The solid line is the numerical D–κ relation.

ρ_0 (g cm^{-3})	c_0 (mm μs^{-1})	q (kJ g^{-1})	C_p (J kg^{-1} K^{-1})	p_{CJ} (GPa)	
1.844	2.339	5.85	1130	36.3	
a	k	v_c (cm^3 g^{-1})	p_c (GPa)	n	b
0.7965	1.30	0.8314	3.738	1.758	0.7
A (mm μs^{-1})	B	C	Z	Γ_r^0	
2.339	2.737	1.45	−0.03076	0.7989	
k_λ (1 μs^{-1})	μ	ν			
110	3.5	0.93			

TABLE 1. Parameters for the WR-EOS calibrated to PBX-9501.

good agreement at small κ, where the asymptotic expansions are strictly valid. There is also very good agreement close to D_{CJ}. The differences increase as κ increases. The turning point in the numerical D–κ relation is at $\kappa_c = 6.03 \times 10^{-3}, D_c = 6.07$. The present formulation yields a turning point at $\kappa_c = 6.30 \times 10^{-3}, D_c = 6.11$ and the turning point calculated in Kasimov & Stewart (2005) is at $\kappa_c = 7.19 \times 10^{-3}, D_c = 6.04$. The asymptotic D–κ relation presented here is in better agreement with the numerical D–κ relation than the asymptotic result obtained in Kasimov & Stewart (2005), since we do not truncate (3.8) to leading order in $\dot{D}$ and κ.

6.3. *Detonation dynamics of PBX-9501*

The WR-EOS and a pressure-dependent rate equation are used to represent PBX-9501 with $Z_2 = \phi = 1$ (no compaction). Table 1 shows the calibrated parameters obtained by Lambert *et al.* (2006). Initial conditions are atmospheric pressure $p_0 = 1 \times 10^{-4}$ GPa, $\rho_0 = 1.844$ g cm^{-3}, $u_0 = 0$ and $\lambda_0 = 0$.

We start by calculating the D–κ relation using $\mathscr{F}(D, \kappa) = 0$ and plot it in figure 2 along with the numerical D–κ relation. As in the case for a hydrogen–oxygen mixture shown in figure 1, the two curves display good agreement close to $\kappa = 0$ and $D = D_{CJ}$,

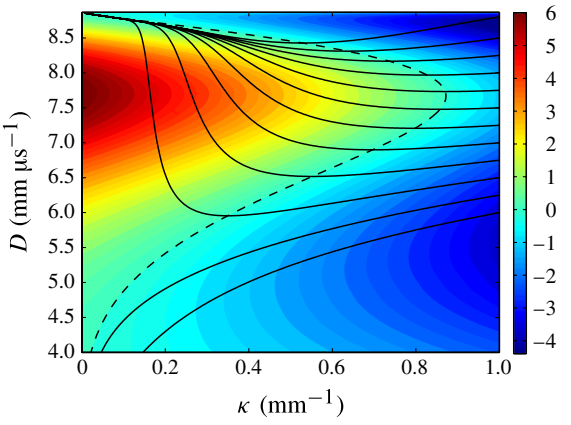

FIGURE 3. Spherical detonation ignition and failure in PBX-9501. Solid lines are the ignition curve solutions to the asymptotic relation $\dot{D} = \mathscr{F}(D, \kappa)$, with initial conditions given by $\kappa_0 = 1$ and D_0 ranging from 8.75 to 6.0 mm μs^{-1} every 0.5 mm μs^{-1}. The dashed line is the asymptotic D–κ relation $\dot{D} = \mathscr{F}(D, \kappa) = 0$. Color contours show values of constant $\dot{D}$ (mm μs^{-2}).

and as κ increases away from $\kappa = 0$ the differences become larger. The upper branch of the D–κ relation obtained with our formulation lies above that of the numerical D–κ relation.

The hydrogen–oxygen model with the set of parameters used in § 6.2 is one-dimensionally unstable and comparisons with DNSs are difficult to carry out. A condensed phase explosive such as PBX-9501 is hydrodynamically stable, allowing comparison against numerical solutions of the reactive Euler equations. The dynamics of ignition events of spherically expanding detonation waves are calculated by solving the initial value problem $\dot{D} = \mathscr{F}(D, \kappa)$ with initial conditions $D(t = 0) = D_0$ and $R(t = 0) = R_0$ using the scheme described in § 5. An embedded Runge–Kutta Prince–Dormand method, as implemented in the GNU Scientific Library (Galassi *et al.* 2009), is used to solve this initial value problem. The ignition transients calculated from the asymptotic formulation are compared with shock-fitted DNSs of the reactive Euler equations computed with the method described by Taylor (2010). These simulations use numerical D–κ solutions as initial conditions. A unique feature of the shock-fitted DNS method is that both $\dot{D}$, D and the shock radius R, which can be related to κ in radially symmetric coordinates, are directly calculated as part of the solution algorithm. In contrast, DNS with shock-capturing numerical methods in the laboratory frame requires an algorithm to locate the lead shock in time. Here D and $\dot{D}$ must be computed numerically from the reconstructed shock trajectory. This produces considerable noise in the results due to the discretization of the grid. For this reason, shock-fitted DNS generates much more accurate values for the measured shock dynamic quantities.

A contour plot of $\dot{D} = \mathscr{F}(D, \kappa)$ is shown in figure 3. The dashed line shows the D–κ relation on which $\dot{D} = \mathscr{F}(D, \kappa) = 0$. The solid lines are ignition curves showing detonation trajectories in the κ–D plane, calculated for $\kappa_0 = 1.0$ and values of D_0 ranging from 8.75 to 6.0 mm μs^{-1} every 0.25 mm μs^{-1}. Here $\dot{D}$ is positive to the left of the D–κ relation and negative to the right. This is reflected in the ignition curves, which have positive slope to the left of the D–κ relation, negative slope to the right of

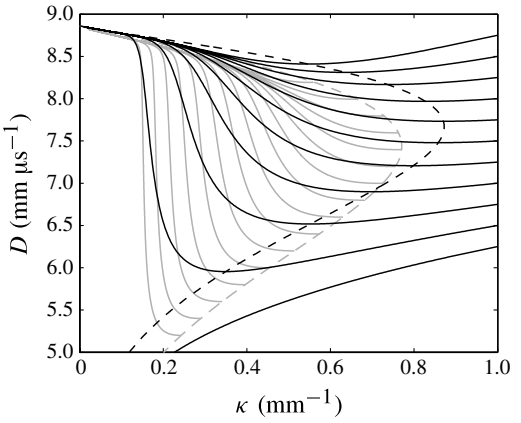

FIGURE 4. Spherical detonation ignition and failure in PBX-9501. Solid grey ignition curves were calculated from DNSs using the shock-attached formulation of the reactive Euler equations with initial conditions obtained from the numerical D–κ relation (dashed grey line). Solid black ignition curves were calculated by solving the asymptotic relation $\dot{D} = \mathscr{F}(D, \kappa)$. Initial conditions for the asymptotic ignition curves are $\kappa_0 = 1$ mm^{-1} and D_0 ranging from 6.25 to 8.75 mm μs^{-1} in increments of 0.25 mm μs^{-1}. Dashed black line is the asymptotic D–κ relation $\dot{D} = \mathscr{F}(D, \kappa) = 0$.

it and zero slope where they cross the D–κ relation. The curves calculated with $D_0 =$ 6.0 and 6.25 mm μs^{-1} fail to ignite, indicating that there is a critical initial velocity D_I (6.25 mm μs^{-1} $< D_I <$ 6.5 mm μs^{-1} for this initial radius that separates successful ignitions from failed ignitions. A successful ignition event can be characterized as follows. A shock with an initial velocity D_0 expands outwards as κ decreases and R increases. During this initial expansion, the energy lost due to divergence, represented by the last term on the right-hand side of the compatibility condition (3.7), is larger than the energy released by reaction, represented by the first term on the right-hand side of (3.7). As the wave continues to expand, the energy contributed by the reaction increases and the energy lost due to flow divergence decreases as κ becomes smaller, causing the magnitude of deceleration to decrease. This continues until the reaction and divergence terms balance out, at which point the wave crosses the D–κ relation with $\dot{D} = 0$. After this point, the wave starts accelerating. The acceleration magnitude increases until the wave approaches the upper branch of the D–κ relation as κ becomes small and R becomes large. The detonation velocity continues to increase, but the rate at which it does so is progressively smaller as D asymptotes to the D–κ relation and approaches D_{CJ}.

Ignition transient curves computed with shock-fitted DNS are shown as solid grey lines in figure 4. The numerical D–κ relation is shown as a grey dashed line. Ignition transient curves calculated using $\dot{D} = \mathscr{F}(D, \kappa)$ are shown in figure 4 as solid black lines, along with the asymptotic D–κ relation calculated by $\dot{D} = \mathscr{F}(D, \kappa) = 0$ shown as a black dashed line. Calculations with DNSs and asymptotics both show that $\dot{D} > 0$ to the left of the corresponding D–κ relation, although the shock acceleration is found to be higher in DNSs.

In the DNSs of ignition events, time derivatives and powers of κ are retained to all orders. A direct comparison of ignition events obtained from DNSs and $\dot{D} = \mathscr{F}(D, \kappa)$ would require initial conditions to be comparable. In the context of this

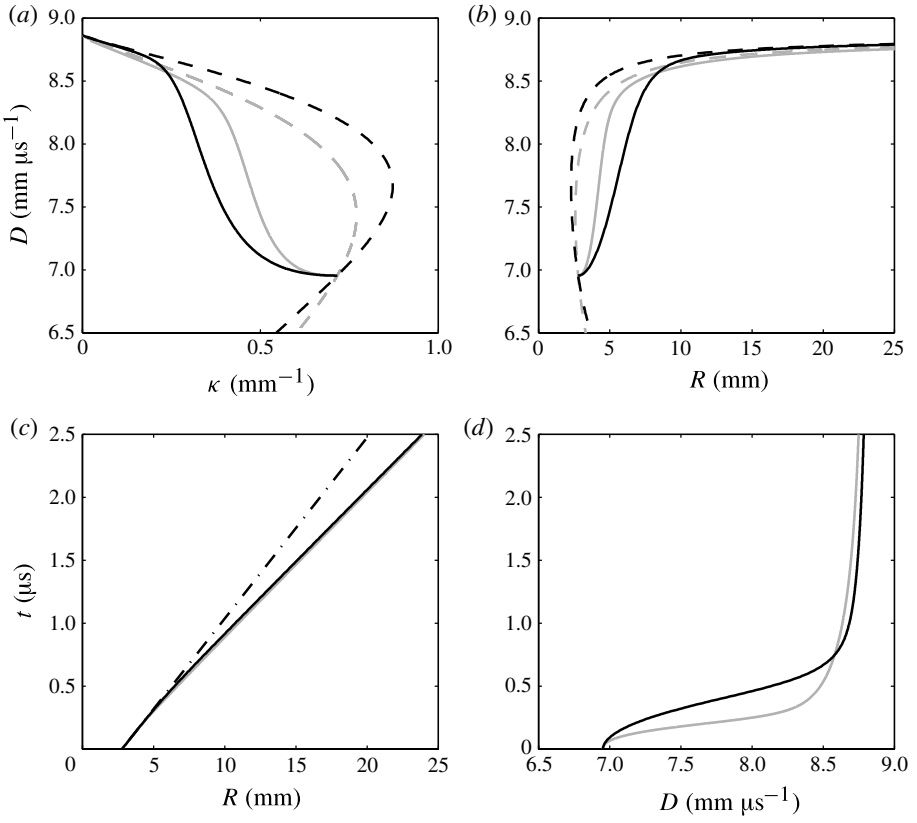

FIGURE 5. Ignition events starting at $D_0 = 6.954$ mm μs^{-1}, $\kappa_0 = 0.7163$ mm^{-1} and $R_0 = 2.7921$ mm. Solid grey and black lines represent results obtained from DNSs and from the asymptotic $\dot{D} = \mathscr{F}(D, \kappa)$ relations, respectively. Dashed lines represent D–κ relations obtained numerically (grey) and from $\mathscr{F}(D, \kappa) = 0$ (black). Detonation speed D is plotted as a function of (*a*) κ and (*b*) R. Position R and detonation speed D are plotted as functions of time in (*c*) and (*d*), respectively. The dash-dot line in (*c*) represents the trajectory of a wave travelling at constant speed D_0.

work, comparable initial conditions should be such that time derivatives $\ddot{D}$ and higher, and higher-order terms than κ, are zero. The closest we can come to these conditions are initial conditions from the intersection of the numerical and $\mathscr{F}(D, \kappa) = 0$ D–κ relations, where $D = 6.954$ mm μs^{-1}, $\kappa = 0.7163$ mm^{-1} and $R = 2.7921$ mm. We use this point to set initial conditions to compare the dynamics and evolution of an ignition event obtained with DNS and $\dot{D} = \mathscr{F}(D, \kappa)$. Figure 5 shows these ignition curves, calculated by DNSs (solid grey line) and by $\dot{D} = \mathscr{F}(D, \kappa)$ (solid black line). In figure 5(*a,b*), the velocity of the shock front D is plotted as a function of κ and R, respectively. Both ignition curves start with no acceleration. After acceleration begins, the acceleration of the detonation wave is higher when calculated using DNSs than by $\dot{D} = \mathscr{F}(D, \kappa)$. Both curves exhibit acceleration buildup, first with positive jerk ($\ddot{D}$) followed by negative jerk as they approach the respective D–κ relations.

The position R and detonation speed D of the wave are plotted as functions of time in figure 5(*c,d*), respectively. Figure 5(*c*) also shows the trajectory of a wave travelling at constant speed $D = 6.954$ mm μs^{-1} as a dash-dot line. Trajectories in the

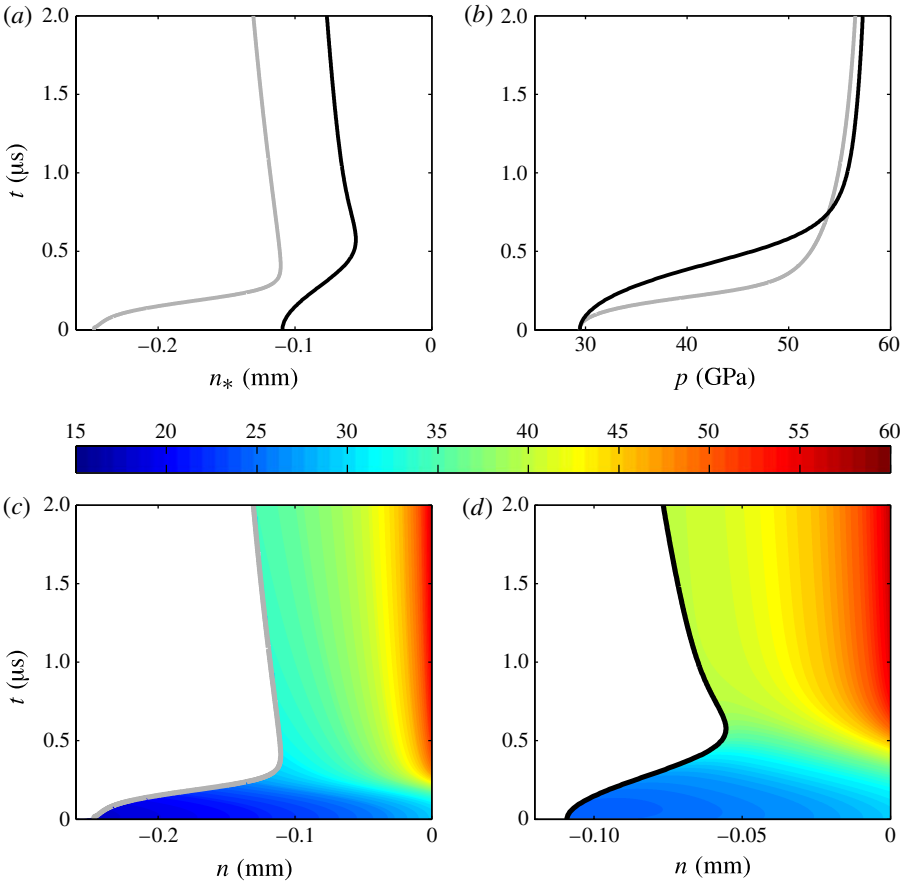

FIGURE 6. Ignition events starting at $D_0 = 6.954$ mm μs^{-1}, $\kappa_0 = 0.7163$ mm^{-1} and $R_0 = 2.7921$ mm. Gray and black lines represent results obtained from DNS and from the asymptotic $\dot{D} = \mathscr{F}(D, \kappa)$ relation, respectively. (*a*) Location of the sonic locus n_* obtained from DNS and $n_{(0)*}$ from the solution to $\dot{D} = \mathscr{F}(D, \kappa)$. (*b*) Pressure at the shock. Pressure field in the region between the shock and (*c*) the sonic locus n_* obtained from DNS and (*d*) the sonic locus $n_{(0)*}$ from the solution to $\dot{D} = \mathscr{F}(D, \kappa)$. The colour scale shows pressure in GPa for (*c*) and (*d*).

R–*t* plane calculated with DNS and with $\dot{D} = \mathscr{F}(D, \kappa)$ are almost indistinguishable for $t \leqslant 0.4$ μs, and slightly differ for $t > 0.4$ μs. The detonation wave travels at velocities in the range $6.954 \text{ mm } \mu\text{s}^{-1} < D < 8.8624 \text{ mm } \mu\text{s}^{-1}$ or $0.785 < D/D_{CJ} < 1.0$. The biggest differences in the detonation velocities calculated by the two methods occur during a short transition time, between $t = 0.05$ μs and $t = 0.7$ μs, for 26 % of the total time shown. For $t < 0.05$ μs and $t > 0.7$ μs, the differences in the detonation velocities are small. By the time the wave calculated with $\dot{D} = \mathscr{F}(D, \kappa)$ gets close to the D–κ relation, $D = 8.68$ mm μs^{-1} (98 % of D_{CJ}), $t = 0.98$ μs (39.2 % of the time simulated) and $R = 10.56$ mm (44.3 % of the total trajectory, namely 23.85 mm).

The structure of the detonation wave as it evolves in time is presented in figure 6. Again, the grey lines represent calculations using DNSs and the black lines represent calculations using the asymptotic $\dot{D} = \mathscr{F}(D, \kappa)$ relation. The evolution of the position

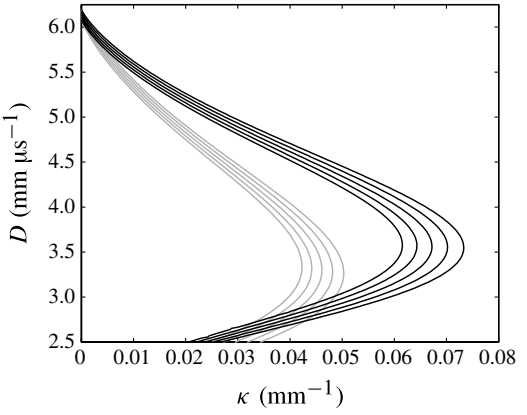

FIGURE 7. The D–κ relations for HMX with $\phi_0 = 1.0, 0.9, 0.8, 0.7$ and 0.6, from right to left. Black lines represent the solution to $\mathscr{F}(D, \kappa) = 0$ and grey lines represent D–κ relations calculated numerically.

of the sonic locus n_* obtained by DNSs and $n_{(0)*}$ obtained from solving $\dot{D} = \mathscr{F}(D, \kappa)$ is shown in figure 6(*a*). The large difference in n_* indicates that this quantity is sensitive to the higher-order terms neglected in the asymptotic formulation. Figure 6(*b*) shows the pressure at the shock, which is calculated using the Rankine–Hugoniot relations and depends on the ambient state and on the detonation velocity D. When the detonation speed calculated with $\dot{D} = \mathscr{F}(D, \kappa)$ is $D = 8.68$, 98 % of D_{CJ}, the difference between the pressure at the shock calculated between the two methods is small. Also shown are plots of the pressure between the shock and n_* calculated by DNSs in figure 6(*c*), and between the shock and $n_{(0)*}$ calculated with $\dot{D} = \mathscr{F}(D, \kappa)$ in figure 6(*d*).

6.4. *Effects of compaction on detonation dynamics in condensed phase explosives*

We perform calculations to show results of our formulation when the two composition variables represent exothermic reaction and endothermic compaction in HMX and PETN.

6.4.1. *HMX granular explosive*

The effect of endothermic compaction is first evaluated for the case of an ideal equation of state (4.7), an Arrhenius reaction rate equation (4.1) and a compaction rate based on a linear quasistatic response (4.3), with parameters that are chosen to be representative of an HMX granular explosive (Stewart *et al.* 1994). Results are shown for spherical geometry ($j = 2$) and parameters $\gamma = 2.0$, $Q_\lambda = 6.4$ kJ g^{-1}, $k_\lambda = 3.35$ μs^{-1}, $\nu = 1.0$, $E_a = 7.296$ kJ g^{-1}, $Q_\phi = 0.6$ kJ g^{-1} and $k_\phi = 1.53$ μs^{-1}, with initial conditions $p_0 = 1 \times 10^{-4}$ GPa, theoretical maximum density $\rho_{TMD} = 1.71$ g cm^{-3}, $u_0 = 0$ and $\lambda_0 = 0$.

Figure 7 shows the asymptotically obtained D–κ relations calculated using $\mathscr{F}(D, \kappa) = 0$ (shown as black lines) and the numerical D–κ relation (shown with grey lines). The values of ϕ_0 are varied from 0.6 on the leftmost curves to 1.0 on the rightmost curves in increments of 0.1. For small curvature near D_{CJ}, the curves calculated with the asymptotic formulation converge to the curves calculated numerically. Differences between the two methods become apparent for larger values

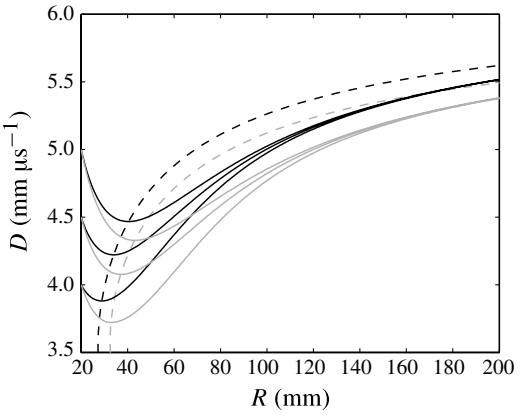

FIGURE 8. Ignition curves obtained by solving the initial value problem $\dot{D} = \mathscr{F}(D, \kappa)$ with initial conditions $R_0 = 20$ mm and $D_0 = 5.0$, 4.5 and 4.0 mm μs^{-1} in HMX with $\phi_0 = 1.0$ (black lines) and $\phi_0 = 0.6$ (grey lines). Also shown are $\dot{D} = \mathscr{F}(D, \kappa) = 0$ curves with $\kappa = 2/R$, represented by dashed lines.

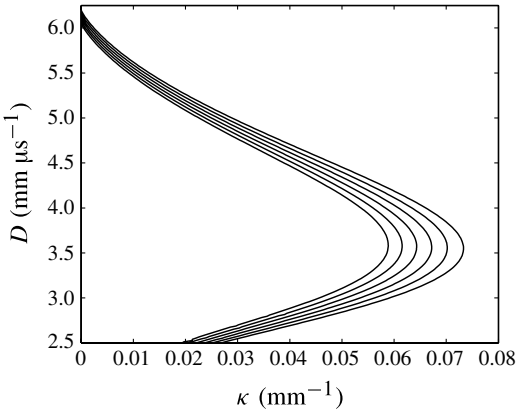

FIGURE 9. D–κ relations obtained by solving $\mathscr{F}(D, \kappa) = 0$ for HMX with $\phi = 0.7$ and Q_ϕ varying from 0 to 1.0 kJ g^{-1} in increments of 0.2 kJ g^{-1}. Q_ϕ increases from right to left.

of κ. However, the qualitative trends for the D–κ relations are the same for both methods as the D–κ relations shift to the left with decreasing values of ϕ_0.

The effects of varying ϕ_0 can also be seen in figure 8, which shows ignition curves for spherically expanding detonations starting at $R_0 = 20$ mm, with $D_0 = 5.0$, 4.5 and 4.0 mm μs^{-1}, and $\phi_0 = 1.0$ (black lines) and $\phi_0 = 0.6$ (grey lines). Also shown are $\dot{D} = \mathscr{F}(D, \kappa) = 0$ curves with $\kappa = 2/R$, displayed as dashed lines. In the D–R plane, lowering ϕ_0 shifts the $\dot{D} = \mathscr{F}(D, \kappa) = 0$ curve to the right in the R axis. As a result, a detonation in HMX with $\phi_0 = 0.6$ decelerates for longer distances and starts accelerating at higher values of R and lower values of D than it does with $\phi_0 = 1.0$ with the same initial conditions R_0 and D_0.

Figure 9 shows the effect of varying compaction energy on the asymptotic D–κ relations for $\phi_0 = 0.7$. As Q_ϕ is increased from 0 to 1.0 kJ g^{-1}, the entire D–κ curve shifts to the left, with the largest change occurring at the upper turning point.

ρ_{TMD} (g cm^{-3})	c_0 (mm μs^{-1})	q (kJ g^{-1})	C_v (J (kg K)$^{-1}$)	p_{CJ} (GPa)	
1.76	2.3	5.71	992	31.5	
a	k	v_c (cm^3 g^{-1})	p_c (GPa)	n	b
0.7579	1.30	1.2171	1.5899	0.9570	0.80
A (mm μs^{-1})	B	C	Z	Γ_r^0	
2.30	2.50	0.70	−0.8066	1.22	
k_λ (μs^{-1})	μ	ν	P_h (GPa)	k_ϕ (GPa^{-1} μs^{-1})	
1200	3.8	0.4	0.07	31.5	

TABLE 2. Parameters for the WR-EOS calibrated to PETN at the theoretical maximum density (TMD).

The CJ detonation velocity D_{CJ} for the ideal equation of state (4.7) is given by

$$D_{CJ} = \sqrt{c_0^2 + q} + \sqrt{q} \tag{6.12}$$

with

$$q = \frac{(\gamma^2 - 1)}{2} \left[Q_\lambda \lambda_* - Q_\phi (\phi_* - \phi_0) \right]. \tag{6.13}$$

Typically, the energy of compaction Q_ϕ is an order of magnitude smaller than the energy of reaction Q_λ, and q is positive. Increasing the energy of compaction Q_ϕ causes q and D_{CJ} to decrease, as occurs in figure 9.

6.4.2. *PETN powders*

In this section, the proposed asymptotic formulation is implemented to calculate the dynamic properties of PETN powders using a non-ideal EOS and reaction and compaction variables with complex rate equations. The model for PETN that will be used here was developed and calibrated by Saenz & Stewart (2008) and is composed of the WR-EOS presented in § 4.3.2, a pressure-dependent reaction rate equation (4.2) and a compaction rate based on the P–α model (4.6). Calibrated parameters for the PETN model are shown in table 2.

Figure 10 shows D–κ relations for PETN calculated using the parameters in table 2 and using the asymptotically formulated $\dot{D}$–D–κ relation $\mathscr{F}(D, \kappa) = 0$ for $\phi_0 = 1.0$ (bold curve), 0.95, 0.9, 0.85, 0.8 and 0.75. Here D_{CJ} decreases with decreasing ϕ_0. The intersection of the D–κ relation with $D = 4$ mm μs^{-1} occurs at increasing values of κ as ϕ_0 decreases. Values of D_c on the turning point (κ_c, D_c) that separates the upper branch and the middle branch decrease with decreasing ϕ_0. The curvature κ_c on the turning point decreases for $\phi_0 = 1.0$, 0.95 and 0.9, and then increases for $\phi_0 = 0.85$, 0.8 and 0.75.

7. Discussion and conclusions

The formulation and calculations presented in this work shed some light onto the nature and character of the dynamics of detonation waves and on the theory of detonation shock dynamics, evolving our understanding of this phenomena. We developed a formulation to calculate asymptotic $\dot{D}$–D–κ relations in materials modelled with general equations of state of the form $e(p, v, Z_i)$ where composition

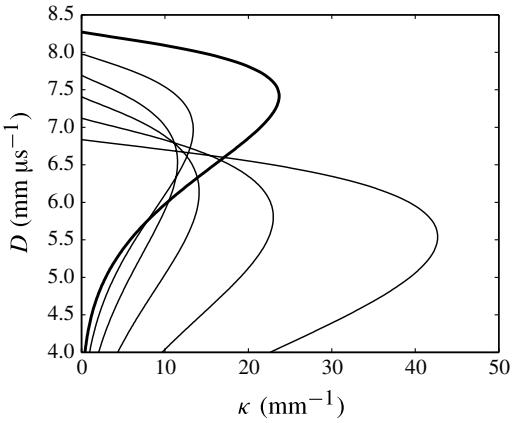

FIGURE 10. The D–κ relations obtained by solving $\mathscr{F}(D, \kappa) = 0$ for PETN with $\phi_0 = 1.0$ (bold curve), 0.95, 0.9, 0.85, 0.8 and 0.75. Here D_{CJ} decreases with decreasing ϕ_0. The intersection of the D–κ relation with $D = 4$ mm μs^{-1} occurs at increasing values of κ as ϕ_0 decreases.

variables Z_i can be used to represent non-equilibrium rate processes such as chemical reactions and compaction processes. The results presented here are the first calculations that develop asymptotic $\dot{D}$–D–κ relations for general material models. This work is partly based on the asymptotic framework used first by Kasimov & Stewart (2005) to calculate an asymptotic $\dot{D}$–D–κ relation for an explosive modelled with an ideal equation of state and an Arrhenius reaction rate. It was demonstrated that retaining additional terms in the sonic boundary condition, thereby avoiding truncation of that condition to $O(\dot{D}, \kappa)$, improved the accuracy of the asymptotic solution.

The present asymptotic formulation was used to model and make comparisons with DNSs of spherical ignition events in condensed phase explosives. Our results indicate that, in general, ignition transients are short lived and rapid. Typically, the time it takes a for a detonation wave to ignite and accelerate to a speed near the upper branch of the D–κ relation is small compared with the time the wave spends close to or on the upper branch. This has important implications for engineering calculations and modelling of detonation dynamics, as it indicates that using a $\dot{D}$–D–κ, or even a D–κ relation, to model the dynamics of a detonation wave is a good approximation and that errors produced by neglecting fast transients are in general small. The calculations presented in this work also illustrate that the location of the sonic locus is very sensitive to higher-order terms in the asymptotic expansions.

The asymptotic results applied to explosive models incorporating compaction, reaction and realistic, non-ideal forms of the equation of state demonstrate that an intrinsic $\dot{D}$–D–κ relation can be determined for most condensed explosives of technological importance. Such a relation can be used to predict detonation front trajectories for engineering applications. The asymptotic analysis is carried out under the assumption that curvature is positive.

Previous work (Stewart 1998; Lambert *et al.* 2006) indicates that it is reasonable to expect that the results presented in this paper (e.g. (6.6)) can be extended to describe the dynamics of overdriven detonations ($D > D_{CJ}$) with negative curvature ($\kappa < 0$) for materials where both exothermic reactions and endothermic compaction occur. To determine the relevant branch of the D–κ relation for negative curvature, the thermicity

condition should be replaced by the condition that $\lambda_* = 1$, while retaining the sonic condition (Stewart 1998). Using the condition $\lambda_* = 1$ is physically sensible because of the dramatic rise of pressure states at the shock that occur in overdriven detonations. This extension has been verified in other contexts using a reactive flow model to both: (*a*) generate an extended D–κ relation that admits negative curvature for $D > D_{CJ}$, and using this D–κ relation to compute the dynamic evolution of a detonation event; and (*b*) comparing this evolution with the shock evolution computed directly from the reactive flow model. These two calculations compare favourably with experiments for the HMX-based explosive PBX-9501 (Lambert *et al.* 2006). In these experiments, only a small section of the detonation front surface has negative curvature, so the overall evolution of the shock is not affected by the section with negative curvature. The extension is thought to be well understood, but the rigorous asymptotic justification of this extension is still under-investigated and *ad hoc*. The extension is beyond the scope of this paper.

Acknowledgements

J.A.S, B.D.T. and D.S.S. were supported by US Air Force Office of Scientific Research Physical Mathematics and Applied Analysis under grant FA9550-06-1-0044 (Program Manager Dr A. Nachman) and US Air Force Research Laboratory Munitions Directorate under grant FA8651-05-1-0003 (Program Manager Dr D. Lambert). B.T. was also supported by the US Department of Energy Computational Science Graduate Fellowship program under grant DE-FG02-97ER25308. Computations were performed, in part, on the UIUC CSE cluster on equipment purchased through US AFOSR DURIP under grant FA9550-06-1-0332. We thank four anonymous reviewers for comments that helped improve that quality of this paper.

Appendix A. Wide-ranging equation of state

The equations used to represent detonation products and reactants in the WR-EOS are included in this appendix. The reader is referred to Wescott *et al.* (2005) for further details.

A.1. *Detonation products*

The energy e_p and pressure p_p for products are expressed as

$$e_p(p, v) = e_p^s(v) + \frac{v}{\Gamma_p(v)}(p - p_p^s(v)) \tag{A 1}$$

and

$$p_p(e, v) = p_p^s(v) + \frac{\Gamma_p(v)}{v}(e - e_p^s(v)), \tag{A 2}$$

where v is the specific volume, the subscript p indicates detonation products and the superscript s indicates that a function is defined on the isentrope passing through the CJ state. The remaining functions are defined as follows

$$p_p^s(v) = p_c \frac{\left[\frac{1}{2}(v/v_c)^n + \frac{1}{2}(v/v_c)^{-n}\right]^{a/n}}{(v/v_c)^{k+a}} \frac{k - 1 + F(v)}{k - 1 + a}, \tag{A 3}$$

$$F(v) = \frac{2a(v/v_c)^{-n}}{(v/v_c)^n + (v/v_c)^{-n}}, \tag{A 4}$$

$$\Gamma_p(v) = k - 1 + (1 - b)F(v), \tag{A 5}$$

$$e_p^s(v) = e_c \frac{\left[\frac{1}{2}(v/v_c)^n + \frac{1}{2}(v/v_c)^{-n}\right]^{a/n}}{(v/v_c)^{k-1+a}}, \tag{A 6}$$

$$e_c = \frac{p_c v_c}{k - 1 + a}, \tag{A 7}$$

where p_c, v_c, a, k, n and b are parameters that are calibrated against experimental data.

A.2. *Detonation reactants*

The equations for energy e_r and pressure p_p of the reactants are

$$e_r(p, v) = e_r^s(v) + \frac{v}{\Gamma_r(v)}(p - p_r^s(v)) \tag{A 8}$$

and

$$p_r(e, v) = p_r^s(v) + \frac{\Gamma_r(v)}{v}(e - e_r^s(v)), \tag{A 9}$$

where the pressure on the principle isentrope is calculated via

$$p_r^s(v) = \hat{p}\left[\sum_{j=1}^{3}\frac{(4By)^j}{j!} + C\frac{(4By)^4}{4!} + \frac{y^2}{(1-y)^4}\right], \tag{A 10}$$

where A and B are determined from shock Hugoniot data from experiments, the subscript r denotes reactants EOS, $y = 1 - v/v_0$ and $\hat{p} = rho_0 A^2/4B$. The remaining functions are defined as follows

$$e_r^s(v) = v_0 \int_0^y p_r^s(\bar{y})\,\mathrm{d}\bar{y} + e_0, \tag{A 11}$$

$$\Gamma_r(y) = \Gamma_r^0 + Zy, \tag{A 12}$$

$$\Gamma_r^0 = \beta c_0^2/C_p, \tag{A 13}$$

$$Z = (\Gamma_{sc} - \Gamma_r^0)/y_{max}, \tag{A 14}$$

$$y_{max} = \frac{2}{\Gamma_p(y_{max} + 2)}, \tag{A 15}$$

where β is the thermal expansion coefficient, C_p is the specific heat at constant pressure and c_0 is the bulk sound speed.

Appendix B. Equations in λ coordinates

To implement our formulation for material models with a reaction progress variable $Z_1 \equiv \lambda$ and a compaction progress variable $Z_2 \equiv \phi$, equations (3.9)–(3.11) are rewritten in λ coordinates using the transformation $\mathrm{d}n = U_{(0)}\,\mathrm{d}\lambda/\omega_{\lambda(0)}$. With this transformation, the fluxes at the sonic locus (3.9) become

$$M_* = M_{(0)*} + M_{(1)*}, \tag{B 1a}$$

$$P_* = P_{(0)*} + P_{(1)*}, \tag{B 1b}$$

$$H_* = H_{(0)*} + H_{(1)*}, \tag{B 1c}$$

$$\phi_* = \phi_{(0)*} + \phi_{(1)*}, \tag{B 1d}$$

where terms $M_{(0)*}$, $P_{(0)*}$, $H_{(0)*}$ and $Z_{i(0)*}$ are obtained as described in § 2.3. The correction terms are given by

$$M_{(1)*} = -\dot{D}I_1 - \kappa M_{(0)*} n_{(0)*} - \kappa D I_0, \tag{B 2a}$$

$$P_{(1)*} = \rho_0 \dot{D} n_{(0)*} - \dot{D} I_0 - \kappa M_{(0)*}^2 J_0 - \kappa M_{(0)*} D n_{(0)*}, \tag{B 2b}$$

$$H_{(1)*} = \frac{-D\dot{D}I_0}{M_{(0)*}} - \dot{D} n_{(0)*} + \frac{\dot{D} S_1}{M_{(0)*}}, \tag{B 2c}$$

$$\phi_{(1)*} = -\dot{D}T - \frac{\dfrac{\partial \phi_{(0)*}}{\partial D}}{U_{(0)*}} \dot{D} n_{(1)*}, \tag{B 2d}$$

with

$$I_0 = \int_0^{\lambda_{(0)*}} \frac{\rho_{(0)} U_{(0)}}{\omega_{\lambda(0)}} \, \mathrm{d}\lambda, \tag{B 3a}$$

$$J_0 = \int_0^{\lambda_{(0)*}} \frac{U_{(0)} v_{(0)}}{\omega_{\lambda(0)}} \, \mathrm{d}\lambda, \tag{B 3b}$$

$$I_1 = \int_0^{\lambda_{(0)*}} \frac{U_{(0)}}{\omega_{\lambda(0)}} \frac{\partial \rho_{(0)}}{\partial D} \, \mathrm{d}\lambda, \tag{B 3c}$$

$$S_1 = \int_0^{\lambda_{(0)*}} \frac{U_{(0)}}{\omega_{\lambda(0)}} \frac{\partial p_{(0)}}{\partial D} \, \mathrm{d}\lambda, \tag{B 3d}$$

$$T = \int_0^{\lambda_{(0)*}} \frac{1}{\omega_{\lambda(0)}} \frac{\partial Z_{i(0)}}{\partial D} \, \mathrm{d}\lambda, \tag{B 3e}$$

$$n_{(0)*} = -D \int_0^{\lambda_{(0)*}} \frac{\mathrm{d}\lambda}{\rho_{(0)} \omega_{\lambda(0)}}, \tag{B 3f}$$

In (B 2*d*) the contributions from the term containing $n_{(1)}*$ is neglected in order to evaluate $\phi_{(1)*}$ to $O(\dot{D}, \kappa)$. With the relations given in (B 1)–(B 3), the compatibility condition (3.7) and the speed relation (3.8) now constitute a relation between $\dot{D}$, D, κ and λ_*.

Appendix C. Numerical solution of the quasisteady DSD equations

The procedure used to obtain D–κ relations numerically is described in this appendix. It is assumed that the material model includes two composition variables, Z_1 and Z_2, to represent reaction and compaction progress, respectively. However, the same general methodology can be applied to models with more or fewer composition variables.

The quasisteady mass, momentum and composition equations obtained from the reduced Euler equations (2.8*a*), (2.8*b*) and (2.8*d*), respectively, are

$$\frac{\mathrm{d}M}{\mathrm{d}n} = -\kappa\rho \left(U + D\right), \tag{C 1}$$

$$\frac{\mathrm{d}P}{\mathrm{d}n} = -\kappa\rho U \left(U + D\right), \tag{C 2}$$

$$\frac{\mathrm{d}Z_1}{\mathrm{d}n} = \frac{\omega_1}{U}, \tag{C 3}$$

$$\frac{\mathrm{d}Z_2}{\mathrm{d}n} = \frac{\omega_2}{U}. \tag{C 4}$$

The mass and momentum equations are combined with the quasisteady energy equation (2.8*c*), $\mathrm{d}H/\mathrm{d}n = 0$, to form the master equation,

$$\frac{\mathrm{d}U}{\mathrm{d}n} = \frac{\Phi}{\eta}. \tag{C 5}$$

The numerical solution algorithm integrates the master equation together with the mass, momentum and composition equations in order to compute the state variables from the fluxes without having to use a nonlinear root solver.

The thermicity condition Φ is given by

$$\Phi = c^2 \sum_{i=1}^{2} \omega_i \sigma_i - \kappa c^2 (U + D) \tag{C 6}$$

where σ_i is the thermicity coefficient of composition variable i defined in (2.12), and ω_i is the rate at which composition variable i changes. The speed relation η is defined as

$$\eta = c^2 - U^2. \tag{C 7}$$

The flux variables at the shock in (2.9*a–d*) are used as boundary conditions at the shock. The boundary conditions in the far field are defined by the values of the thermicity condition and the speed relation at the sonic locus, namely

$$\Phi_* = \eta_* = 0, \tag{C 8}$$

where subscript $*$ indicates terms evaluated at the sonic locus.

The system of equations (C 4)–(C 5) along with boundary conditions (2.9*a–d*), (C 6) and (C 7) constitute a nonlinear eigenvalue problem for κ given D and the ambient state. Given an equation of state $e(p, v, Z_i)$, expressions for the rate of change of the composition variables $\omega_i(p, v, Z_j)$ and the ambient state, the eigenvalue problem is fully specified. The solution algorithm proceeds as follows:

(i) read D;
(ii) set κ_{min} and κ_{max}, such that $\kappa_{min} < \kappa < \kappa_{max}$;
(iii) set $\kappa_{tmp} = (\kappa_{min} + \kappa_{max})/2$;
(iv) integrate (C 5)–(C 4) from the shock to the far field, until one of these conditions is met:
  (*a*) $\eta_* = 0$,
  (*b*) Φ goes from positive to negative or
  (*c*) counter reaches maximum number of integration steps allowed;
(v) if $\eta_* = 0$, set κ_{min} to κ_{tmp};
(vi) if Φ went from positive to negative, set κ_{max} to κ_{tmp};
(vii) if reached maximum number of integration steps, return an error message and stop;
(viii) if $(\kappa_{max} - \kappa_{min}) < \epsilon_{abs} + \epsilon_{rel} \max(\kappa_{min}, 0)$, stop;
(ix) go to step (iii).

The algorithm described above will either return an interval $\kappa_{min} \leqslant \kappa \leqslant \kappa_{max}$ guaranteed to contain the solution κ within the specified tolerances ϵ_{abs} and ϵ_{rel} or an error message indicating that too many steps were taking during the integration.

REFERENCES

BDZIL, J. B. & STEWART, D. S. 2007 The dynamics of detonation in explosive systems. *Annu. Rev. Fluid Mech.* **39** (1), 263–292.

BDZIL, J. B. & STEWART, D. S. 2011 *Theory of Detonation Shock Dynamics. Detonation Dynamics* (ed. F. Zhang). *Shock Wave Science and Technology Reference Library*, vol. 6, chap. 7. Springer.

DAVIS, W. C. 1985 Equation of state for detonation products. In *Proceedings of the 8th (International) Detonation Symposium*, pp. 785–795.

DAVIS, W. C. 1993 Equation of state for detonation products. In *Proceedings of 10th International Symposium on Detonation*, pp. 369–376.

DAVIS, W. C. 1998*a* Equation of state for detonation products. In *Proceedings of 11th International Symposium on Detonation*, pp. 303–308.

DAVIS, W. C. 1998*b* Explosive effects and applications. In *Introduction to Explosives*, chap. 1. Springer.

DAVIS, W. C. 2000 Complete equation of state for unreacted solid explosive. *Combust. Flame* **120**, 399–403.

GALASSI, M., DAVIES, J., THEILER, J., GOUGH, B., JUNGMAN, G., ALKEN, P., BOOTH, M. & ROSSI, F. 2009 *GNU Scientific Library Reference Manual*, 3rd edn. Network Theory Ltd.

HERRMANN, W. 1969 Constitutive equation for the dynamic compaction of ductile porous materials. *J. Appl. Phys.* **40** (6), 2490–2499.

KASIMOV, A. R. 2004 Theory of instability and nonlinear evolution of self-sustained detonation waves. PhD thesis, University of Illinois Urbana-Champaign, Urbana, Illinois.

KASIMOV, A. R. & STEWART, D. S. 2004 On the dynamics of self-sustained one-dimensional detonations: a numerical study in the shock-attached frame. *Phys. Fluids* **16**, 3566–3578.

KASIMOV, A. R. & STEWART, D. S. 2005 Asymptotic theory of evolution and failure of self-sustained detonations. *J. Fluid Mech.* **525**, 161–192.

LAMBERT, D. E., STEWART, D. S., YOO, S. & WESCOTT, B. L. 2006 Experimental validation of detonation shock dynamics in condensed explosives. *J. Fluid Mech.* **546**, 227–253.

MENIKOFF, R. & PLOHR, B. J. 1989 The Riemann problem for fluid flow of real materials. *Rev. Mod. Phys.* **61** (1), 75.

SAENZ, J. A. & STEWART, D. S. 2008 Modelling deflagration-to-detonation transition in granular explosive pentaerythritol tetranitrate. *J. Appl. Phys.* **104** (4), 043519.

STEWART, D. S. 1998 The shock dynamics of multidimensional condensed and gas phase detonations. *Proc. Combust. Inst.* **27**, 2189–2205.

STEWART, D. S., ASAY, B. W. & PRASAD, K. 1994 Simplified modelling of transition to detonation in porous energetic materials. *Phys. Fluids* **6**, 2515–2534.

STEWART, D. S. & BDZIL, J. B. 1988 The shock dynamics of stable multidimensional detonation. *Combust. Flame* **72** (3), 311–323.

STEWART, D. S., DAVIS, W. C. & YOO, S. 2002 Equation of state for modelling the detonation reaction zone. In *Proceedings of 12th Intl Symp. Detonation*, pp. 624–631. Office of Naval Research, ONR 333-05-2.

STEWART, D. S. & KASIMOV, A. R. 2005 Theory of detonation with an embedded sonic locus. *SIAM J. Appl. Maths* **66** (2), 384–407.

STEWART, D. S. & YAO, J. 1998 The normal detonation shock velocity-curvature relationship for materials with nonideal equation of state and multiple turning points. *Combust. Flame* **113** (1–2), 224–235.

STEWART, D. S., YOO, S. & WESCOTT, B. L. 2007 High order numerical simulation and modelling of the interaction of energetic and inert materials. *Combust. Theor. Model.* **11** (2), 305–332.

TAYLOR, B. D. 2010 Instability of steady and quasi-steady detonations. PhD thesis, University of Illinois Urbana-Champaign, Urbana, Illinois.

WESCOTT, B. L., STEWART, D. S. & DAVIS, W. C. 2005 Equation of state and reaction rate for the condensed-phase explosives. *J. Appl. Phys.* **98**, 053514.

XU, S. & STEWART, D. S. 1997 Deflagration to detonation transition in porous energetic materials: a model study. *J. Engng Maths* **31**, 143–172.

YAO, J. & STEWART, D. S. 1996 On the dynamics of multi-dimensional detonation. *J. Fluid Mech.* **309**, 225–275.